Available online at www.sciencedirect.com
SCIENCE DIRECT®
Journal of Solid State Chemistry 179 (2006) 349–354
JOURNAL OF SOLID STATE CHEMISTRY
www.elsevier.com/locate/jssc

Effects of hydrothermal post-treatment on microstructures and morphology of titanate nanoribbons

Huogen Yu, Jiaguo Yu*, Bei Cheng, Minghua Zhou

State Key Laboratory of Advanced Technology for Material Synthesis and Processing, Wuhan University of Technology, Luoshi Road 122#, Wuhan 430070, PR China

Received 6 September 2005; received in revised form 17 October 2005; accepted 20 October 2005
Available online 22 November 2005

Abstract

Titanate nanoribbons were prepared via a hydrothermal treatment of rutile-type TiO_2 powders in a 10 M NaOH solution at 200 °C for 48 h. The as-prepared titanate nanoribbons were then hydrothermally post-treated at 150 °C for 12–36 h. The titanate nanoribbons before and after hydrothermal post-treatment were characterized with FESEM, XRD, TEM, UV–VIS and nitrogen adsorption–desorption isotherms. The results showed that the hydrothermal post-treatment not only promoted the phase transformation from titanate to anatase TiO_2, but also was beneficial to the removal of Na^+ ions remained in the titanate nanoribbons. After hydrothermal post-treatment, the TiO_2 samples retained the one-dimensional structure feature of the titanate nanoribbons and showed an obvious increase in the specific surface area and the pore volume.

Keywords: Titanate nanoribbons; Hydrothermal post-treatment; Microstructures; Morphology; Anatase; Phase transformation; Na^+ ions

1. Introduction

One-dimensional (1D) nanomaterials, such as nanotubes, nanowires, nanoribbons and nanorods, have attracted considerable attention recently due to their unique physical and chemical properties and potential applications in constructing nanoscale electronic and photoelectronic devices [1–3]. Of such 1D nanomaterials, TiO_2-based nanotubes or nanofibers have been intensively investigated for their applications in photovoltaic cells, photocatalysis, catalytic supports, and gas sensing [4–6]. Crystalline TiO_2 nanotubes or nanofibers were usually synthesized using porous anodic alumina as templates [7–11]. However, the prepared nanotubes or nanofibers by the above method generally have large diameters (>50 nm) due to the confinement of the molds used. Moreover, the template method often encounters difficulties in the prefabrication and post-removal of the templates and usually results in impurities for the obtained nanomaterials. Further development of synthetic methods is required. Recent studies have indicated that hydrothermal route is a powerful and promising strategy for the preparation of 1D nanomaterials due to its simple procedures and low cost [12–17].

In this study, titanate nanoribbons were prepared via a hydrothermal treatment of rutile-type TiO_2 powders in a 10 M NaOH solution at 200 °C for 48 h, followed by washing with HCl solution and distilled water. The as-prepared titanate nanoribbons were then hydrothermally post-treated in pure water at 150 °C for 12–36 h. The titanate nanoribbons before and after hydrothermal post-treatment were characterized with FESEM, XRD, TEM, UV–VIS and nitrogen adsorption–desorption isotherms. The effects of hydrothermal post-treatment on the microstructures and morphology of the titanate nanoribbons were investigated and discussed.

2. Experimental section

2.1. Preparation of rutile TiO_2 powders

For the preparation of rutile TiO_2 powders, titanium tetraisopropoxide (TTIP, $Ti(OC_3H_7)_4$, 97%) was used as a titanium source. Hydrolysis was carried out at room

*Corresponding author. Fax: +86 27 8787 9468.
E-mail address: jiaguoyu@yahoo.com (J. Yu).

0022-4596/$ - see front matter © 2005 Elsevier Inc. All rights reserved.
doi:10.1016/j.jssc.2005.10.024

temperature by adding 50 ml of TTIP slowly to 1000 ml of distilled water under vigorous stirring for 120 min, followed by aging at room temperature for 12 h in order to further hydrolyze the TTIP. After aging, the gel precipitate was filtered, washed and dried in a vacuum oven at 80 °C for 8 h and then ground into fine powders to obtain xerogel sample. The xerogel sample was calcined at 900 °C in air for 2 h. The specific surface area and the average crystalline size of the obtained rutile TiO_2 were 0.56 m^2/g and over 200 nm, respectively.

2.2. Preparation of titanate nanoribbons

Titanate nanoribbons were prepared using a chemical process similar to that described by Kasuga et al. [12,13]. In a typical synthesis, 1.5 g of rutile-type TiO_2 powder was mixed with 140 ml of 10 M NaOH solution, followed by hydrothermal treatment of the mixture at 200 °C in a 200 ml Teflon-lined stainless steel autoclave for 48 h. After the hydrothermal reaction, the precipitate was dispersed in distilled water by sonication to obtain homogeneous reaction product. Such reaction product was separated by filtration, and then washed with a 0.1 M HCl aqueous solution and distilled water until the pH value of the rinsing solution reached ca. 6.5, corresponding to the pH value of the distilled water. The washed samples were dried in a vacuum oven at 80 °C for 8 h.

2.3. Hydrothermal post-treatment of titanate nanoribbons

In a typical hydrothermal post-treatment, 0.55 g of the as-prepared titanate nanoribbons were mixed with 80 ml of distilled water, followed by a hydrothermal post-treatment of the mixture at 150 °C in a 100 ml Teflon-lined stainless steel autoclave for 12–36 h. After the hydrothermal post-treatment, the obtained samples were filtered and dried in a vacuum oven at 80 °C for 8 h.

2.4. Characterization

Morphology observation was performed on a JSM-6700F field emission scanning electron microscope (FESEM, JEOL, Japan). The X-ray diffraction (XRD) patterns were obtained on a D/MAX-RB X-ray diffractometer (Rigaku, Japan) using Cu$K\alpha$ irradiation at a scan rate (2θ) of 0.05° s^{-1} and were used to determine the identity of any phase present and their crystallite size. The accelerating voltage and the applied current were 15 kV and 20 mA, respectively. Transmission electron microscopy (TEM) analyses were conducted with a JEM-2010FEF electron microscope (JEOL, Japan), using 200 kV accelerating voltage. The UV–VIS spectra were obtained on an UV–Visible spectrophotometer (UV-2550, SHIMADZU, Japan). $BaSO_4$ was used as a reflectance standard in the UV–VIS diffuse reflectance experiment. Nitrogen adsorption–desorption isotherms were obtained on an ASAP 2020 (Micromeritics Instruments, USA) nitrogen adsorption apparatus. All the samples were degassed at 100 °C prior to BET measurements. The Brunauer–Emmett–Teller (BET) specific surface area (S_{BET}) was determined by a multipoint BET method using the adsorption data in the relative pressure (P/P_0) range of 0.05–0.25. Desorption isotherm was used to determine the pore size distribution using the Barret–Joyner–Halender (BJH) method [18]. The nitrogen adsorption volume at the relative pressure (P/P_0) of 0.970 was used to determine the pore volume and the average pore size.

3. Results and discussion

Fig. 1a shows the SEM image of well-isolated nanoribbons with a length range from several micrometers to several tens of micrometers and a width of 30–300 nm. A typical image of belt-like structure was shown in Fig. 1b, indicating a high aspect ratio (the width to the thickness) of 3–15 for the as-prepared titanate nanoribbons. The XRD pattern of the nanoribbons (Fig. 2a) showed a feature similar to that of alkali or hydrogen titanates such as $H_2Ti_3O_7$ [14], $Na_xH_{2-x}Ti_3O_7$ [17], or $Na_yH_{2-y}Ti_nO_{2n+1}\cdot xH_2O$ [19] due to a similar structure of layered titanate family.

XRD result indicated that only anatase phase was obtained after the titanate nanoribbons were hydrothermally post-treated at 150 °C for 24 h (as shown in Fig. 2b). The SEM images showed that the obtained TiO_2 powders appeared a rod-like morphology (Figs. 1c and 1d). Therefore, the crystalline anatase TiO_2 retained the 1D feature of the titanate nanoribbons after hydrothermal post-treatment, though the length of the obtained TiO_2 samples was shortened and some rounded TiO_2 particles were found to be attached on the surface of rod-shaped TiO_2 particles.

Figs. 3a and b show the TEM and HRTEM images of the titanate nanoribbons, respectively. An obvious layered structure could be observed in the titanate nanoribbons and the layer spacing was about 0.8 nm (Fig. 3a), corresponding to the diffraction peak located at ca. 11° in Fig. 2a. After hydrothermal post-treatment of the titanate nanoribbons at 150 °C for 24 h, no layered structure was found in the obtained powder samples (Figs. 3c and d) and the samples showed an obvious crystal structure of anatase TiO_2 (Fig. 2b). It should be noted that the titanate and anatase TiO_2 show some similar structure features. In titanium oxide lattice, a TiO_6 octahedron in anatase phase shares four edges with other octahedrons to form a zigzag ribbon structure, while in rutile phase, a TiO_6 octahedron shares edges with other two octahedrons to form linear TiO_6 chains that then links to each other by sharing vertices to obtain three-dimensional lattices [20]. As for the titanate lattice, in addition to the four edge-sharing TiO_6 octahedra and the zigzag ribbon structures similar to that of the anatase TiO_2, the zigzag ribbons then form a titanate layer by sharing the corners of these ribbons and the protons or sodium ions can exist between the titanate layers [21,22]. Therefore, the common features

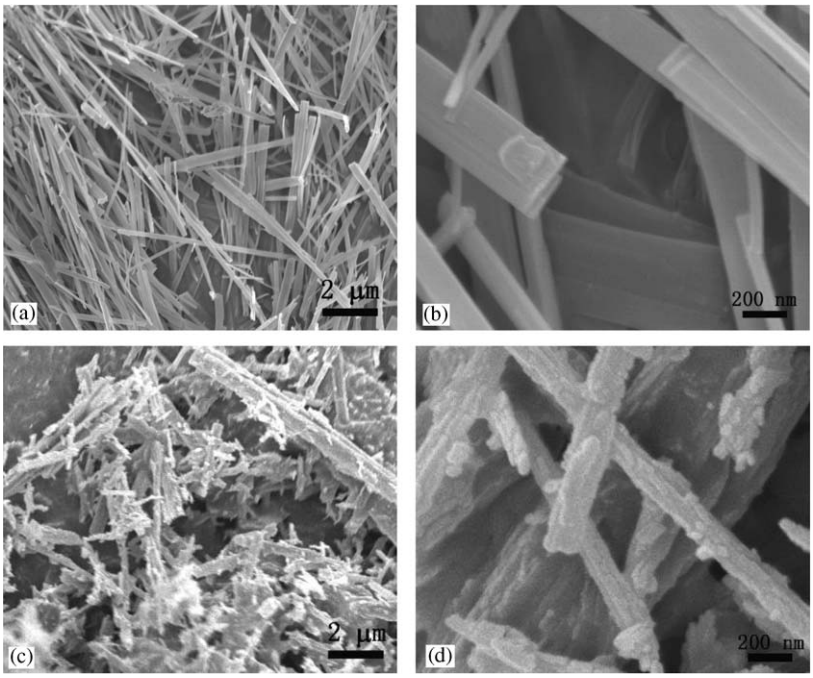

Fig. 1. FESEM images of the titanate nanoribbons before (a and b) and after (c and d) hydrothermal post-treatment at 150 °C for 24 h.

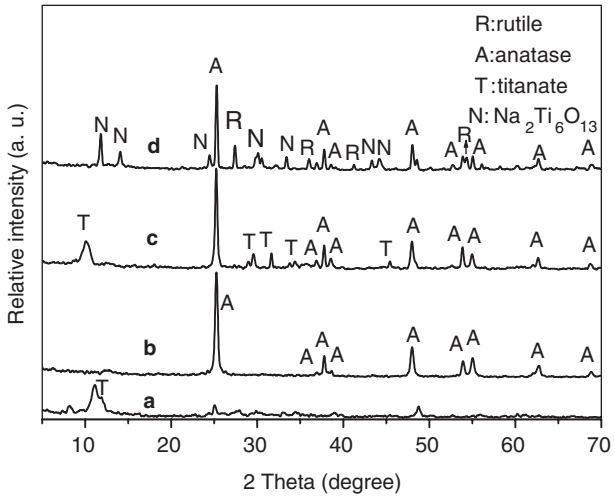

Fig. 2. XRD patterns of the as-prepared titanate nanoribbons (a), nanoribbons hydrothermally post-treated at 150 °C for 24 h (b) and 12 h (c) and nanoribbons calcined at 700 °C for 2 h (d).

of crystal structures of anatase and titanate revealed that it was easier to form anatase TiO_2 than to obtain rutile phase by the dehydration among the layers in the titanate nanoribbons. It was suggested that the dehydration process among the titanate layers was accompanied by an in-situ rearrangement of the structural unites (such as the zigzag ribbons), and the phase transition from titanate to anatase was a topochemical reaction process which had a low energy requirement to break the bonding in titanate [23]. Thus, the anatase phase could be obtained by the hydrothermal post-treatment of titanate at 150 °C.

When the hydrothermal post-treatment time was reduced to 12 h, the diffraction peaks of both anatase and titanate could be observed in the reaction products (Fig. 2c), indicating a partial phase transition of the titanate. Further observation indicated that the diffraction peak corresponding to the gallery spacing of the layered titanate shifted to the left at ca. 9° after the hydrothermal post-treatment of titanate nanoribbons for 12 h. The shift of diffraction peaks suggested a different gallery spacing of the powder samples obtained at different hydrothermal post-treatment time. This can be ascribed to the distortion or destruction of the layered structure in the titanate due to the dehydration because the dehydration among the titanate layers leads to the change of gallery spacing. Further experimental investigation indicated that the Na^+ ions could not be completely removed by acid washing with an HCl solution due to a thick belt-shaped structure of the as-prepared titanate. This could be confirmed by heating the washed nanoribbons at 700 °C for 2 h. It was found that in addition to the anatase and rutile TiO_2, the diffraction peaks of titanate $Na_2Ti_6O_{13}$ (JCPDS NO. 37-0951) were also observed (Fig. 2d). On the contrary, there was no sodium titanate observed in the TiO_2 samples obtained by hydrothermal post-treatment of the same samples at 150 °C for 24 h (Fig. 2b). Therefore, it was reasonable to suggest that the H^+ or H_3O^+ ions in the reaction system could enter the titanate layers and substitute the Na^+ ions remained in the titanate nanoribbons and hydrothermal treatment enhanced the substitution of the Na^+ ions and the formation of anatase TiO_2. Though the K^+ or Na^+ ions in the titanates, such as $K_2Ti_4O_9$, $Na_2Ti_4O_9$, could be exchanged by H^+ ions using

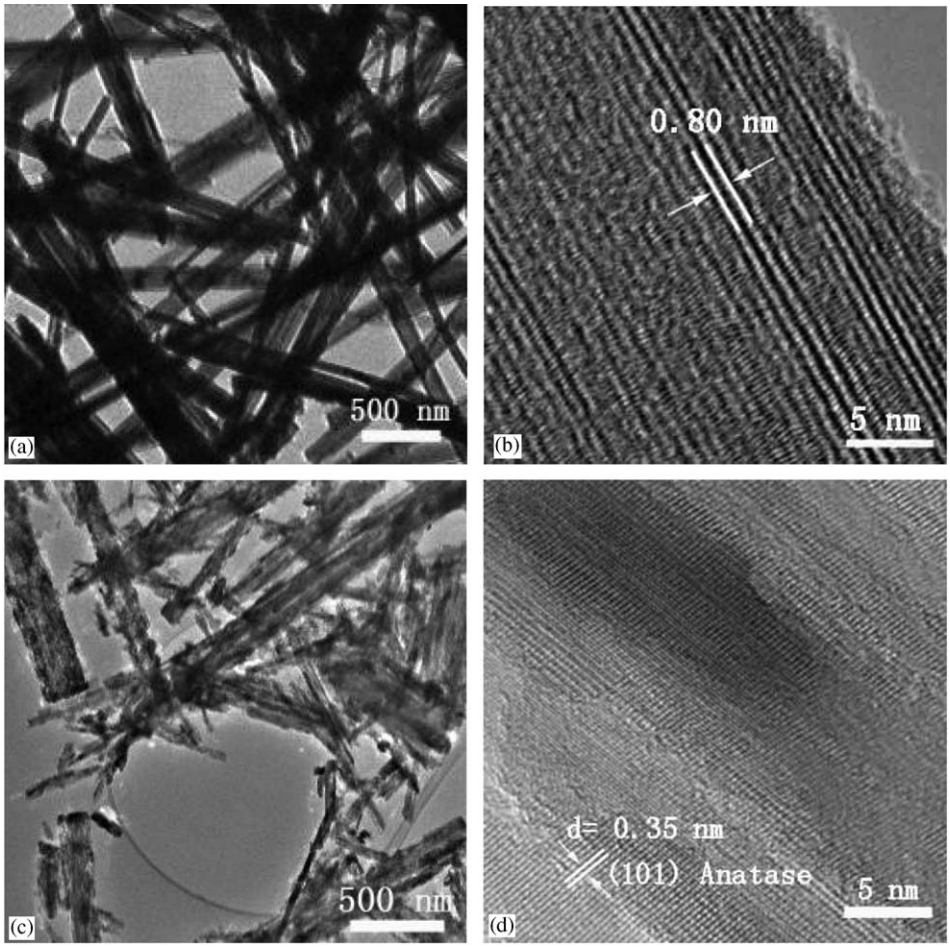

Fig. 3. TEM and HRTEM images of the as-prepared titanate nanoribbons (a and b) and crystalline anatase TiO_2 powders prepared by hydrothermal post-treatment of the titanate nanoribbons at 150 °C for 24 h (c and d).

HCl or HNO_3 aqueous solution, the resulted samples were the titanate $H_2Ti_4O_9$ instead of crystalline anatase or rutile TiO_2 [24,25]. In this case, in order to obtain anatase TiO_2, the titanate $H_2Ti_4O_9$ was usually calcined or hydrothermally treated. However, the obtained crystalline TiO_2 by the above methods was not a pure anatase phase, usually containing monoclinic TiO_2 or rutile phase [25]. Therefore, here, the removal of the Na^+ ions remained in the titanate nanoribbons was different from the usual ion exchange of Na^+ ions with H^+ ions reported in the previous studies. It could be seen from the above results that the elimination of the Na^+ ions was accompanied by the dehydration of titanate and the phase transformation from titanate to anatase TiO_2. Our previous research results showed that Na^+ ions had an obvious deleterious effect on the photocatalytic activity of TiO_2 samples [26,27]. Such a hydrothermal route could provide a new insight into the elimination of the Na^+ ions existed in TiO_2 photocatalyst.

Fig. 4 shows the nitrogen adsorption–desorption isotherms and their corresponding pore size distributions of titanate nanoribbons before and after hydrothermal post-treatment for 24 h. It can be seen that all the samples show a type H3 hysteresis loop according to IUPAC classification [18], indicating the presence of mesopores (2–50 nm). Moreover, the observed hysteresis loop approaches $P/P_0 = 1$, suggesting the presence of macropores (>50 nm) [28].

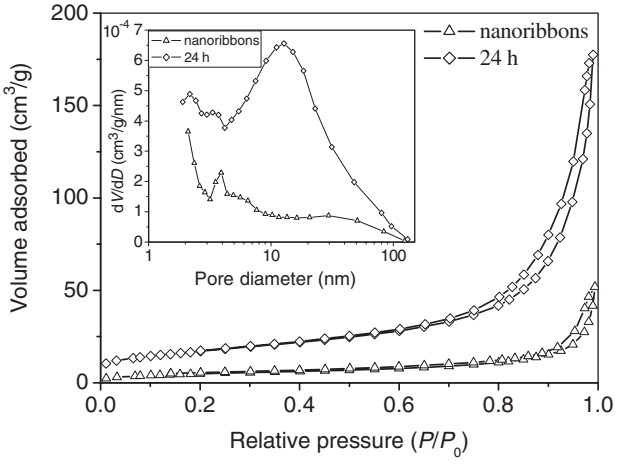

Fig. 4. The nitrogen adsorption–desorption isotherms and their corresponding pore size distributions (inset) of the titanate nanoribbons before and after hydrothermal post-treatment at 150 °C for 24 h.

The pore size distributions (inset) indicate a wide distribution range from 2 to over 100 nm. The pore volume of the titanate nanoribbons and crystalline anatase TiO_2 samples are 0.04 and 0.19 cm^3/g, respectively, determined at the relative pressure (P/P_0) of 0.970. In fact, the titanate nanoribbon does not contain mesopores (>2 nm). Therefore, the existing mesopores (or pore volume) can be attributed to the formation of the aggregates of titanate nanoribbons. After hydrothermal post-treatment for 24 h, a higher pore volume was due to the aggregations of TiO_2 particles with smaller size and the pores formed by the dehydration of the titanate layers. The S_{BET} of titanate nanoribbons and anatase TiO_2 samples, calculated by a multipoint BET method using the adsorption data in the relative pressure (P/P_0) range of 0.05–0.25, are 18.3 and 61.6 m^2/g, respectively. The higher S_{BET} of the anatase TiO_2 powders obtained after hydrothermally post-treatment can be attributed to the formation of short rod-shaped and small rounded TiO_2 particles (as shown in Fig. 3c). Moreover, an obvious increase in mesopore volume also resulted in the increase of S_{BET} of the TiO_2 sample.

Hydrothermal post-treatment obviously affected the light absorption characteristics of the titanate nanoribbons, as shown in Fig. 5. A significant increase in the absorption at wavelengths less than 400 nm can be assigned to the intrinsic band gap absorption of the samples [29]. With increasing hydrothermal post-treatment time, the absorption edge of the samples shows an obvious red shift. This can be attributed to the difference in both compositions and phase structures of the samples. To further explain the effect of the hydrothermal post-treatment time on the red shift, the band gap energies can be estimated from a plot of $(h\nu\alpha)^{1/2}$ versus photo energy ($h\nu$). The intercept of the tangent to the plot will give a good approximation of the indirect band gap energies of the samples. The relation between the absorption coefficient (α) and incident photon energy ($h\nu$) can be written as $\alpha = B_i(h\nu - E_g)^2/h\nu$, where B_i is absorption constants for indirect transitions [30,31]. Since absorbance (A) is proportional to absorption coefficient (α), we use absorbance (A) to substitute absorption coefficient (α) [31]. The plots of $(Ah\nu)^{1/2}$ versus $h\nu$ are presented in Fig. 6. The band gap energy for the titanate nanoribbons was estimated to be 3.08 eV, which was very close to the reported value of 3.1 eV for titanate nanotubes [17]. After hydrothermal post-treatment of the titanate nanoribbons, the band gap energies decreased slightly. The titanate nanoribbons obtained by hydrothermal post-treatment for 12 h showed the lowest band gap energy of 2.93 eV. This may be related to the partial phase transition of titanate nanoribbons. When the hydrothermal post-treatment time was greater than 24 h, the band gap energy (ca. 3.04 eV) of the samples had not an obvious change, indicating the formation of the crystalline anatase TiO_2 powders. Though the value is lower than the reported value for anatase (3.2 eV) [32], it is close to the calculated value of 2.91 eV for indirect band gap energy [33]. The different band gap energies can be attributed to the difference in the preparation method and the surface microstructures of the TiO_2 sample [34].

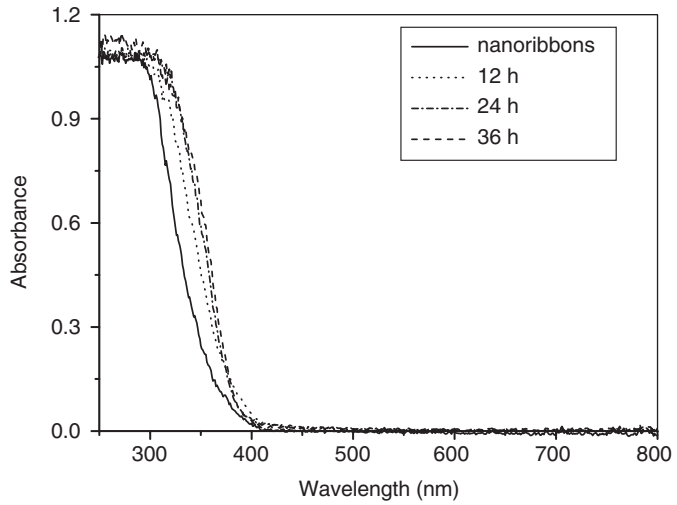

Fig. 5. UV–VIS spectra of titanate nanoribbons before and after hydrothermal post-treatment at 150 °C for 12, 24, and 36 h.

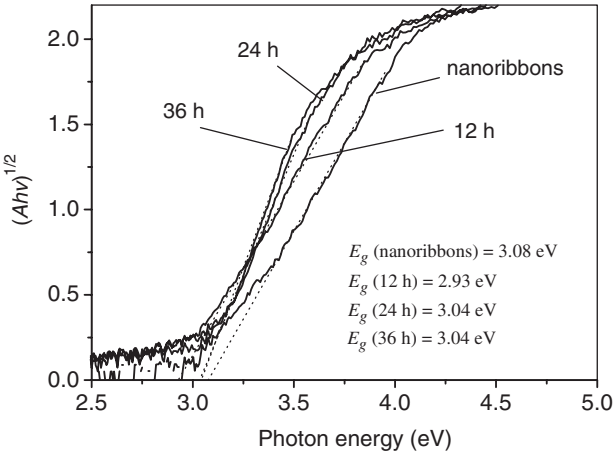

Fig. 6. Plots of $(Ahv)^{1/2}$ versus photon energy ($h\nu$) for the titanate nanoribbons before and after hydrothermal post-treatment at 150 °C for 12, 24, and 36 h. A in the Y-axis title represents absorbance, which is proportional to absorption coefficient (α) [30].

4. Conclusions

In summary, hydrothermal post-treatment obviously affected the microstructures and morphology of the titanate nanoribbons. The hydrothermal post-treatment not only promoted the phase transformation from titanate to anatase TiO_2, but also was beneficial to the removal of Na^+ ions remained in the titanate. After hydrothermal post-treatment, the resulted anatase TiO_2 samples showed an obvious increase in the specific surface area and the pore volume.

Acknowledgments

This work was partially supported by the National Natural Science Foundation of China (50272049 and 20473059). This work was also financially supported by the Excellent Young Teachers Program of MOE of China and Project-Sponsored by SRF for ROCS of SEM of China.

References

[1] G. Patzke, F. Krumeich, R. Nesper, Angew. Chem. Int. Ed. 41 (2002) 2446.
[2] C.N.R. Rao, M. Nath, Dalton Trans. (2003) 1.
[3] J.G. Yu, J.C. Yu, W.K. Ho, L. Wu, X.C. Wang, J. Am. Chem. Soc. 126 (2004) 3422.
[4] D.Y. Zhang, L.M. Qi, Chem. Commun. (2005) 2735.
[5] S.Z. Chu, S. Inoue, K. Wada, D. Li, H. Haneda, S. Awatsu, J. Phys. Chem. B 107 (2003) 6586.
[6] O.K. Varghese, D.W. Gong, M. Paulose, K.G. Ong, E.C. Dickey, C.A. Grimes, Adv. Mater. 15 (2003) 624.
[7] P. Hoyer, Langmuir 12 (1996) 1411.
[8] S.M. Liu, L.M. Gan, L.H. Liu, W.D. Zhang, H.C. Zeng, Chem. Mater. 14 (2002) 1391.
[9] S. Lee, C. Jeon, Y. Park, Chem. Mater. 16 (2004) 4292.
[10] H. Imai, Y. Takei, K. Shimizu, M. Matsuda, H. Hirashima, J. Mater. Chem. 9 (1999) 2971.
[11] Y. Lei, L.D. Zhang, G.W. Meng, G.H. Li, X.Y. Zhang, C.H. Liang, W. Chen, S.X. Wang, Appl. Phys. Lett. 78 (2001) 1125.
[12] T. Kasuga, M. Hiramatsu, A. Hoson, T. Sekino, K. Niihara, Langmuir 14 (1998) 3160.
[13] T. Kasuga, M. Hiramatsu, A. Hoson, T. Sekino, K. Niihara, Adv. Mater. 11 (1999) 1307.
[14] Q. Chen, W.Z. Zhou, G.H. Du, L.M. Peng, Adv. Mater. 14 (2002) 1208.
[15] B.D. Yao, Y.F. Chan, X.Y. Zhang, W.F. Zhang, Z.Y. Yang, N. Wang, Appl. Phys. Lett. 82 (2003) 281.
[16] Z.Y. Yuan, W. Zhou, B.L. Su, Chem. Commun. (2002) 1202.
[17] X.M. Sun, Y.D. Li, Chem. Eur. J. 9 (2003) 2229.
[18] K.S.W. Sing, D.H. Everett, R.A.W. Haul, L. Moscou, R.A. Pierotti, J. Rouquerol, T. Siemieniewska, Pure Appl. Chem. 57 (1985) 603.
[19] J. Canales, P.G. Bruce, Angew. Chem. Int. Ed. 43 (2004) 2286.
[20] H. Izawa, S. Kikkawa, M. Koizumi, J. Phys. Chem. 86 (1982) 5023.
[21] J.K. Brudett, T. Hughbanks, G.J. Miller, J.W. Richardson, J.V. Smith, J. Am. Chem. Soc. 109 (1987) 3639.
[22] H.Y. Zhu, Y. Lan, X.P. Gao, S.P. Ringer, Z.F. Zheng, D.Y. Song, J.C. Zhao, J. Am. Chem. Soc. 127 (2005) 6730.
[23] H.Y. Zhu, X.P. Gao, Y. Lan, D.Y. Song, Y.X. Xi, J.C. Zhao, J. Am. Chem. Soc. 126 (2004) 8380.
[24] H. Izawa, S. Klkkawa, M. kolzuml, J Phys. Chem. 86 (1982) 5023.
[25] S. Yin, S. Uchida, Y. Fujishiro, M. Aki, T. Sato, J. Mater. Chem. 9 (1999) 1191.
[26] J.C. Yu, J.G. Yu, J.C. Zhao, Appl. Catal. B 36 (2002) 31.
[27] J.G. Yu, X.J. Zhao, Mater. Res. Bull. 36 (2001) 97.
[28] C.C. Tsai, H. Teng, Chem. Mater. 16 (2004) 4352.
[29] J.C. Yu, J.G. Yu, W.K. Ho, Z.T. Jiang, L.Z. Zhang, Chem. Mater. 14 (2002) 3808.
[30] N. Serpone, D. Lawless, R. Khairutdinov, J. Phys. Chem. 99 (1995) 16646.
[31] X.H. Wang, J.G. Li, H. Kamiyama, M. Katada, N. Ohashi, Y. Moriyoshi, T. Ishigaki, J. Am. Chem. Soc. 127 (2005) 10982.
[32] H. Tang, K. Prasad, R. Sanjines, P.E. Schmid, F. Levy, J. Appl. Phys. 74 (1994) 2042.
[33] N. Daude, C. Gout, C. Jouanin, Phys. Rev. B 15 (1977) 3229.
[34] M.S. Sander, M.J. Cote, W. Gu, B.M. Kile, C.P. Tripp, Adv. Mater. 16 (2004) 2052.